

Structural, Field Emission and Ammonia Gas Sensing Properties of Multiwalled Carbon Nanotube-Graphene Like Hybrid Films Deposited by Microwave Plasma Enhanced Chemical Vapor Deposition Technique

Atul Bisht¹, S. Chockalingam¹, O. S. Panwar^{1,*}, A. K. Kesarwani¹, Ishpal¹, B. P. Singh², and V. N. Singh³

¹Polymorphic Carbon Thin Films Group, Physics of Energy Harvesting Division, ²Physics and Engineering of Carbon, Materials Physics and Engineering Division, ³Electron and Ion microscopy, Sophisticated and Analytical Instruments, CSIR-National Physical Laboratory, New Delhi-110012, India

ABSTRACT

This paper reports the direct deposition of multiwalled carbon nanotube (MWCNT)-graphene like hybrid films on nickel substrate using a 2.45 GHz microwave plasma enhanced chemical vapor deposition (MW PECVD) system in the temperature range of 500–700 °C at 20 Torr pressure. The films have been characterized by Raman spectra, high resolution transmission electron microscope (HRTEM), scanning electron microscope, high resolution X-ray diffraction and contact angle measurement. Raman spectroscopy and HRTEM reveal the formation of MWCNT and graphene like hybrid carbon sheet structures. The effect of processing temperature on the field emission properties of MWCNT-graphene like hybrid films has been investigated. Field emission measurement reveals that the turn-on field decrease and the emission current density increase with the increase of deposition temperature. The rambutan structure of MWCNT formed at 700 °C is responsible for the improvement in the field emission properties. The film deposited at 700 °C shows fast response and recovery time of 40 and 96 s, respectively, for ammonia gas sensing due to the high surface area of the film. It has also been found that the hydrophobic surface of the film helps to perform the gas sensing in the humid environment.

KEYWORDS: MWCNT, Graphene, Hybrid Film, MW PECVD, Field Emission, Raman Spectroscopy, Ammonia Gas Sensing.

1. INTRODUCTION

Recently, sp^2 hybridized carbon based nanostructures such as carbon nanotube (CNT) and graphene have emerged as a subject of intense research due to their unique chemical, electrical, mechanical and thermal properties.^{1–6} Graphene is a two dimensional sheet composed of sp^2 bonded carbon atoms arranged in a honeycomb structure, whereas, CNT is one dimensional rolled graphene sheets. Due to the high surface to volume ratio, capability to be grown on the flexible substrates and unique geometry, both the carbon allotropes are promising candidates for the gas and chemical sensing applications. Recently, carbon based hybrid materials composed of graphene and CNT attracted much attention.^{7–9} The hybrid material contains extraordinary

properties of both the graphene as well as CNT. CNTs are generally grown by pre-seeding the grown substrate by catalyst metal nanoparticles.^{10,11} These metallic nanoparticles remain on the top of the CNT as residues which are not desirable for their applications in many areas like field emitter, super capacitor, electrode for lithium ion battery etc., where there is a need of proper adhesion between the CNT and the substrate. In addition, CNT growth involves a two-step deposition process viz. deposition of first catalytic nanoparticles on the desired substrate and then the growth of the CNT deposition with a suitable precursor. The two step process can be reduced to a single step by directly synthesizing multiwalled carbon nanotube (MWCNT) on the bulk substrate. Many reports suggest that the CNT, graphene and CNT-graphene based hybrid materials are promising for field emission application due to their high aspect ratio, sharp edges and high conductive nature with sp^2 bonded carbon channels,

* Author to whom correspondence should be addressed.

Email: ospanwar@mail.nplindia.ernet.in

Received: XX XXXX XXXX

Accepted: XX XXXX XXXX

etc.^{12,13} Such hybrid material can be grown by different techniques such as chemical vapor deposition (CVD),^{7,8} microwave plasma enhanced CVD (MW PECVD),¹¹ radio frequency plasma enhanced CVD (RF PECVD),¹² sputtering¹³ and chemical based methods.¹⁴

CNT and graphene sensors for gas sensing applications are of significant interest due to their tunable electrical and chemical properties.^{15–17} Generally, sensors based on CNT and graphene are fabricated by using patterning and post electrode deposition with the help of lithography which increase the production cost. The process described in the present work involves the easy and cost effective deposition of electrodes without any lithography process. Ammonia is widely used for different industrial applications such as fertilizer, cleaner, fermentation, precursor for nitrogenous compound, as antimicrobial etc., but it is a highly toxic, corrosive and hazardous gas.^{15–17} Even a very low concentration can kill the aquatic animals and affect the respiratory system, skin, etc. Thus, the detection and quantification of ammonia gas is an important issue for the environmental conditions. Although, metal oxides based gas sensors are commercially used for ammonia detection but they require a high operating temperature (200–400 °C),¹⁸ which may limit their lifetime and performance. Besides the high operating temperatures of the conventional sensors, humidity is another crucial factor which affects the performance of the sensing device. The remedy of these two problems, to grow a hydrophobic material with room temperature sensing response, is the main center of attention for the present study. The hydrophobic nature of the sensing material may help to maintain its sensitivity in the high humidity conditions. Some et al.¹⁹ have studied the hydrophilic and hydrophobic graphene for the high sensitive and selective gas sensing. Hydrophobic membrane is also used to protect the sensor from the fluid and allow sensing material to pass. Though, a simple drop cast method is the easiest method but it is difficult to control the layout of nanomaterial. CNT based film may be a solution for uniform layout and base resistance.¹⁶ One advantage of CNT based sensors is that it can absorb ammonia gas from the water.²⁰

This work reports the structural, field emission and ammonia gas sensing properties of MWCNT-graphene like hybrid films deposited directly on nickel substrate using the MW PECVD technique at different temperatures and fixed 20 Torr pressure. The effect of process temperature (500, 600 and 700 °C) on the surface morphology and field emission properties of hybrid films has been studied. Further, the hydrophobic nature of the film for water repelling properties of sensor has been investigated. The sensor shows a better response and recovers time measured at room temperature which is correlated with their field emission behavior. The field emission and ammonia gas sensing property have been dominantly contributed by the MWCNT-graphene like hybrid films.

2. EXPERIMENTAL DETAILS

2.1. Sample Preparation

MWCNTs-graphene like hybrid films were synthesized on cleaned nickel foil in a custom designed and indigenously built MW PECVD system as shown in Figure 1. It consists of 1.2 KW microwave power supply, magnetron, circulator and three stub tuners. Microwave is coupled to the deposition chamber with a waveguide and a quartz window. Impedance matching is carried out using three stub tuners. The deposition chamber is equipped with a turbo molecular-rotary pump combination and a base pressure of $\sim 3 \times 10^{-7}$ Torr is achieved in the system. The temperature of heating stage was raised with the heating rate of 30 °C/min. When the desired temperature was obtained, the sample was further cleaned by flowing H₂ gas in the chamber to further remove the surface oxide from the nickel substrate. After 10 min of cleaning, the chamber was processed with Ar gas and the pressure was increased to 1 Torr. Argon plasma was first generated using low power. Subsequently, the pressure was increased up to the desired deposition pressure using H₂ and CH₄ gas which was kept at 20 Torr in the present study using a throttle valve. Samples were deposited at different temperatures of 500, 600 and 700 °C. The deposition conditions have been summarized in Table I. After the deposition, the sample was cooled down to room temperature with the natural cooling.

2.2. Characterization

The surface morphology of the sample was examined by the scanning electron microscope (JEOL-JSM-7500 F SEM). For HRTEM study, samples were prepared by etching nickel in HNO₃ + HF mixture and collecting the remaining film after diluting the mixture with the distilled water on the carbon coated copper grid. HRTEM studies were carried out using a Tecnai G20, F-30-ST WIN with field emission electron gun source operated at the electron accelerating voltage of 300 KV. The Raman spectroscopy of these samples was performed using 514 nm excitation

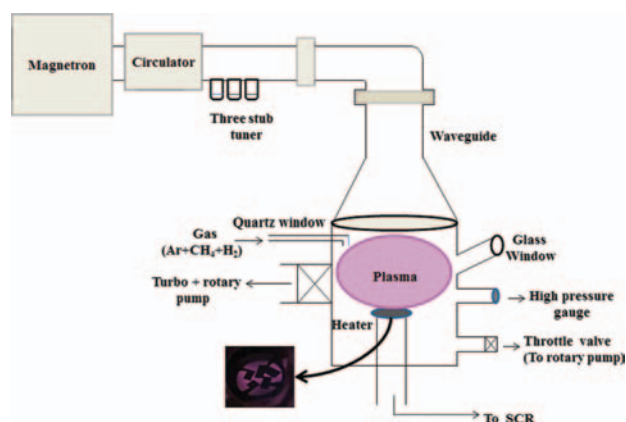


Fig. 1. Schematic diagram of MW PECVD system.

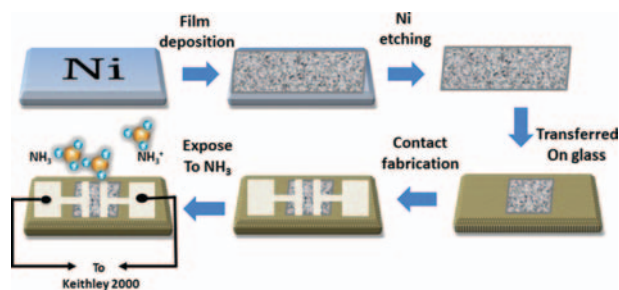
Table I. Various parameters of MWCNT-graphene like hybrid films evaluated from the Raman spectra.

S. no.	Properties/Parameter	500 °C	600 °C	700 °C
1	D (cm^{-1})	1350.3	1340.7	1368.3
2	G (cm^{-1})	1587.5	1597.5	1592.5
3	2D (cm^{-1})	2694.5	2641.2	2728.9
4	D + G (cm^{-1})	2939.0	2933.2	2954.9
5	I_D/I_G	1.73	0.88	0.73
6	I_{2D}/I_G	0.19	0.28	0.26
7	FWHM_{2D} (cm^{-1})	201.3	116.2	147.8

laser using 25 mW/cm^2 incident power and notch filter at $\sim 50 \text{ cm}^{-1}$ at room temperature by a Renishaw spectrophotometer (micro-Raman model in Via Reflex). The structure of the samples was further confirmed by Grazing angle x-ray diffraction which was recorded with PANalytical X'PERT PRO MRD, θ - 2θ and ω -scans. The wavelength of X-ray used was 1.54 \AA with incident angle of 0.5° and 2θ was scanned from 10° to 90° .

The field emission measurements were carried out with a diode configuration directly on nickel substrate as cathode and indium tin oxide (ITO) coated glass as anode. It consists of a stainless steel vacuum chamber pumped by a turbomolecular-rotary pump combination, a high voltage source meter (Keithley, Model 2410) with computer interface using a Labview program that communicates with the Keithley source meter through an IEEE connection. The separation between the anode and the cathode is defined by the PTFE spacer of thickness $\sim 150 \text{ }\mu\text{m}$ and the overlap area between the plate anode and cathode was kept at $\sim 0.196 \text{ cm}^2$. The current-voltage (I-V) characteristics were measured at room temperature under a vacuum $\sim 3 \times 10^{-7}$ Torr. The emission current density (J) was calculated by dividing the emission current (I) by the area of the cathode which is defined by the area of the hole in the spacer. The electric field (E) is defined by the voltage drop across the vacuum gap.

Fabrication of the sensor is depicted in Figure 2. The thermally evaporated silver (Ag) electrode with the dimension of $5 \text{ mm} \times 2 \text{ mm}$ was deposited on the MWCNT-graphene like hybrid film supported on glass with a parallel electrode arrangement with a separation of about 1 mm by using the shadow mask. The sensing response of the prepared structure has been recorded in both the inert (nitrogen) as well as air environment at room temperature in a fully automated system of the film by using Keithley's 2000 digital multimeter and Aalborg mass flow controller (MFC). Initially, the sensor was exposed to nitrogen gas for 10 min to make the sensor resistance stable and then exposed to the ammonia gas diluted with nitrogen for 200 s to measure the sensing signal. The recovery of the sample was tested by flushing the chamber by the nitrogen for 300 s. Similar gas sensing measurements have also been performed in air ambient at different ppms of ammonia. These gas sensing measurements were performed in

**Fig. 2.** Schematic diagram of the sensor fabrication.

a small cell of volume about 100 ml, where the flows of both the analyte (ammonia) as well as diluents (nitrogen/air) gases were controlled by the MFCs. A pre-diluted ammonia gas with dry nitrogen procured from the scientific company (Sigma gases, Pvt. Ltd) was further diluted as per the requirement of ppm levels. To make the 50, 100, 150, 200, 250 and 300 ppm levels of ammonia, a flow of 2, 4, 6, 8, 10 and 12 ml/min of ammonia at 10000 ppm, respectively, was injected by one MFC and 400 ml/min of diluent by another MFC. (Here, $50 \text{ ppm} = (2 \text{ ml/min} \times 10000 \text{ ppm})/400 \text{ ml/min}$). All the measurements were carried out at room temperature.

3. RESULTS AND DISCUSSION

3.1. Raman Spectroscopy

Raman spectroscopy is widely used to study the electronic and molecular structure of carbon and thereby differentiate various forms of carbon based allotropes. Figure 3 shows the Raman spectra of the MWCNT-graphene like hybrid films deposited at different temperatures of (a) 500, (b) 600 and (c) 700 °C. All the samples show the characteristic peaks identified as D, G, 2D and D+G peak. The G peak originates due to the E_{1g} bond stretching of pair of sp^2 bonded carbon atoms either in the ring or chain arrangement and D band is the disorder induced peak which originates due to A_{1g} breathing mode of sp^2 carbon atoms in aromatic ring.^{21,22} The disorder may originate due to the presence of edges, sp^3 bonded carbon atoms, impurities, vacancies etc.²³ Peak around $2500\text{--}2800 \text{ cm}^{-1}$ mainly exists in the sp^2 hybridized carbon allotropes e.g., graphite, CNT, graphene etc. which originates due to the double phonon resonance process.²⁴ The intensity ratio of I_D/I_G and I_{2D}/I_G give the crucial information about the presence of defects and the number of layers in graphene sheets, respectively. Table I summarizes the different parameters of I_D/I_G , I_{2D}/I_G and full width at half maximum of 2D peak (FWHM_{2D}) along with G, D, 2D and D+G peak positions calculated from the Raman spectra by Lorentzian fitting as shown in Figure 3(d). CNT generally shows the G peak at 1580 cm^{-1} and shifting of G peak towards the higher wavenumber of the film deposited at higher temperatures (600 and 700 °C) indicates the presence of graphitic sheets in the samples. It is clear from the Table I

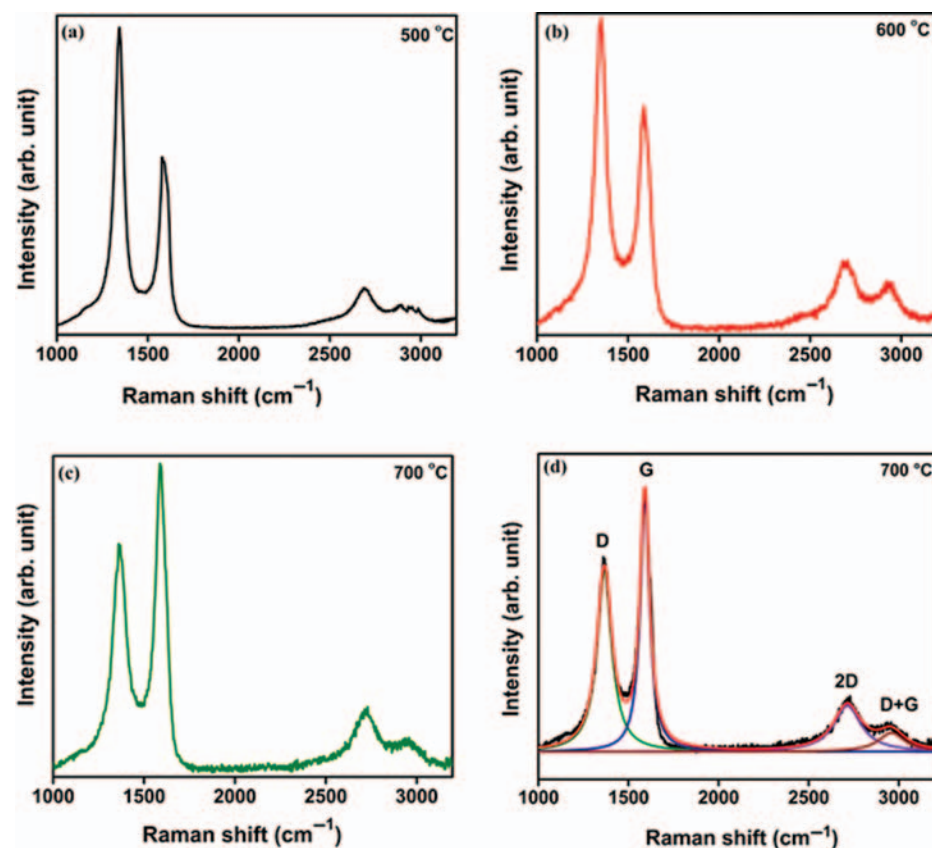


Fig. 3. Raman spectra of MWCNT-graphene like hybrid films deposited at different temperatures of (a) 500, (b) 600, (c) 700 °C, and (d) Lorentzian fitting of Raman spectrum of MWCNT-graphene like hybrid film deposited at 700 °C.

that the I_D/I_G ratio decreases with the increase of deposition temperature, which suggests the decrease in disorder with the increase in the deposition temperatures from 500 to 700 °C. The value of I_{2D}/I_G ratio is found to be 0.19, 0.28 and 0.26 for the MWCNT-graphene hybrid films deposited at different temperatures of 500, 600 and 700 °C, respectively, which shows a maximum value of I_{2D}/I_G at 600 °C deposition temperature. The value of FWHM_{2D} is found to be in the range 116.2–201.3 cm^{-1} . The MWCNT-graphene hybrid film deposited at 600 °C has the lowest value of FWHM_{2D} (116.2 cm^{-1}) accompanied with the highest value of I_{2D}/I_G (0.28). Thus, it can be stated that the formation of MWCNT-graphene like hybrid nature is more at the deposition temperature of 600 °C compared to other deposition temperatures of 500 and 700 °C. Figure 4 shows the Raman mapping of 2D peak over 2500 μm^2 scanned areas for the sample deposited at 600 °C, which shows the uniformity of the sample. A peak around 2900 cm^{-1} appears due to the combined effect of D and G peak and this originates due to the damaged graphitic sheets.²² It is evident from Figure 3 that D+G peak is nearly absent for the deposition temperature of 500 °C.

3.2. XRD Spectra

Figure 5 shows the typical XRD pattern of the MWCNT-graphene like hybrid film deposited at 600 °C on nickel

substrate. A sharp and intense peak at $\sim 26.6^\circ$ in the XRD pattern shows the graphitic nature of the hybrid film. Perfect hexagonal graphite shows a peak at $2\theta = 26.555^\circ$ corresponding to (002) plane (JCPDF no-898497). Interlayer spacing can be calculated from the Bragg's equation:

$$d = \lambda / 2 \sin \theta \quad (1)$$

where d is the interlayer spacing between the crystal plane, θ is the angle of incidence and λ is the wavelength of incident X-ray (1.54 Å). The interlayer spacing evaluated from equation 1 is found to be 0.334 nm which is close to the interlayer spacing of bulk graphite (0.335 nm).

3.3. Surface Microstructural Analysis by SEM and HRTEM Studies

Figure 6 shows the SEM micrograph of the MWCNT-graphene like hybrid films deposited at different temperatures of (a) 500, (b) 600 and (c) 700 °C. Generally, the growth of 1D nanomaterials e.g., nanowire, CNT needs catalyst nanoparticle to grow on the basis of the tip or base growth model. In the present study, no catalyst nanoparticle or any substrate pretreatment has been used to grow nucleation center. Figure 6(a) shows the MWCNT growth at the deposition temperature of 500 °C, showing low density growth. Figure 6(b) shows highly dense

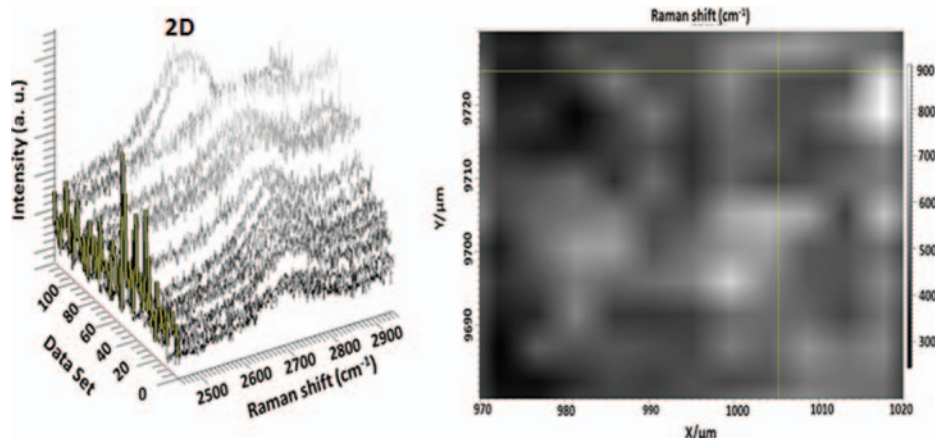


Fig. 4. Raman mapping of 2D peak in MWCNT-graphene like hybrid film deposited at 600 °C temperature.

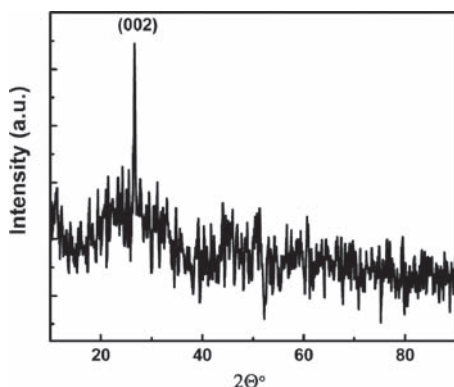


Fig. 5. Typical grazing incidence XRD spectra of MWCNT-graphene like hybrid film deposited at 600 °C temperature.

MWCNT spread all over the substrate at the deposition temperature of 600 °C. Figure 6(c) shows clustering of MWCNT in the flowered like structure at the deposition temperature of 700 °C. The clustering of MWCNT in such a manner is an interesting phenomenon. Tong et al.²⁵ have also found such a uniform and typical rambutan (tree bearing spiny red fruit) like nanostructure on octahedral nickel oxide (NiO) in the powder form and proposed that initially carbon atoms absorbed on octahedral NiO particle reduces them into Ni. Carbon atoms diffused through nickel and MWCNT are grown by the tip growth model. The octahedral NiO crystal plays an important role in the growth of such structures. Such rambutan like nanostructure has

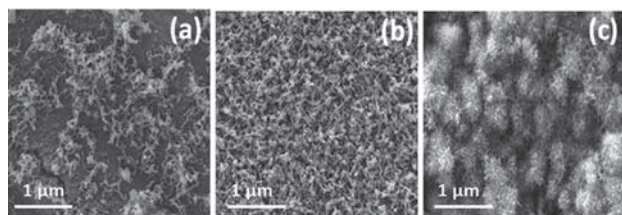


Fig. 6. Typical SEM image of MWCNT-graphene like hybrid films deposited at different temperatures of (a) 500, (b) 600, and (c) 700 °C.

been grown in the present study without any predefined precursor on plane Ni foil. No Ni nanoparticles are seen on the MWCNT tip as revealed by the HRTEM image. Since no pretreatment of the substrate has been performed, the growth may be considered on the basis of pre nucleation of graphitic nanocrystals which acts as a seed for the growth of carbon nanotubes. The growth of these nanocrystals is found to be temperature dependent, which affects the growth of MWCNT. At low temperature, the lower nucleation density of seeding nanocrystals reduces the density of MWCNT's. At high temperature, the density of seeding nanocrystals is high, which results in dense MWCNT's formation. Besides of MWCNTs, graphene sheets also appear at high temperature. At high temperature, graphene sheets are produced due to the diffusion and segregation of carbon atoms on nickel foil.²⁶ Generally, amorphous carbon changes into graphite at high temperature (from 2500–3500 °C) in the absence of a catalyst, whereas in the presence of a catalyst (Ni), it transforms into graphitic at low temperature (from 600–900 °C).²⁵ This is a post MWCNT deposition phenomenon, where first MWCNTs are deposited on nickel substrate with some carbon atoms diffused to nickel foil. After MWCNT is deposited, substrate is cooled very fast by shutting off the power to the heater. With this fast cooling, some carbon atoms segregate to the surface followed by the graphene deposition in some areas. This is also confirmed by the Raman spectra and HRTEM image of the sample. The clustering of MWCNT as flowered structure is also an interesting observation having applications in the field emission, gas sensing, etc., due to its unique structure. Notably, MWCNT along with the thick graphene sheets are visible in the HRTEM image of sample deposited at 700 °C as shown in Figure 7. In the SEM micrograph, graphene sheets may not be visible due to the high density of CNTs. As we etched the nickel surface and observe in HRTEM micrograph, graphene like sheets and CNTs are clearly visible. The MWCNT part has been encircled in the image in Figures 7(a) and (b) shows the low magnification HRTEM

image of the graphene sheet like structure. The fast Fourier transform (FFT) also confirms the crystalline nature of the film. Figure 7(c) depicts the interplaner distance of planes generated using digital micrograph provided by the Gatan software. The interplaner distance of about 0.33 nm has been observed, which is slightly less than the interplaner distance for graphite (0.34 nm) corresponding to d spacing of $\langle 002 \rangle$ plane evaluated from the XRD spectra in Section 3.2.

3.4. Field-Emission

Figure 8 shows the variation in field emission current density (J) versus electric field (E) characteristics of the MWCNT-graphene like hybrid films deposited at different temperatures of (a) 500, (b) 600 and (c) 700 °C. Field-emission is a quantum-mechanical phenomenon in which electrons tunnel out of the electrodes into a vacuum when subjected to a very high electric field. It is a non-linear process, in which the J-E characteristics are usually described by the classical Fowler-Nordheim (FN) equation:²⁷

$$J = \frac{A(\beta E)^2}{\Phi} \exp\left(\frac{-B\Phi^{3/2}}{\beta E}\right) \quad (2)$$

where J is the current density, ϕ is the barrier height (taken as the work function), E is the applied electric field, β is the field enhancement factor and A and B are constants and have the values of $1.54 \times 10^{-6} \text{ AV}^{-2}$ and $6.83 \times 10^9 \text{ Vm}^{-1}\text{eV}^{-3/2}$, respectively. The plots of $\log(J/E^2)$ versus

$1/E$ are shown in Figure 8(d). These plots are straight lines which confirm that the J-E characteristics follow the FN relation. The slopes of these plots give the effective emission barriers ϕ , if we assume an ideal plane emitter with a field enhancement factor β of 1. The values of ϕ calculated for the carbon based films were $\leq 0.1 \text{ eV}$.²⁸⁻³⁰ These values are obviously quite low and the true barrier may be quite large.²⁸ If we consider a work function (ϕ) of 5 eV, typical of graphite bonding then the FN plots correspond to the field enhancement factor β of 1250–3214 for these MWCNT-graphene like hybrid films. The turn-on field (E_T) (corresponding to $1 \mu\text{A}/\text{cm}^2$ emission current density) on MWCNT-graphene like hybrid film has been found to be 4.7, 3.6 and 2.7 $\text{V}/\mu\text{m}$ at different temperatures of 500, 600 and 700 °C, respectively. The values of J at 3.8 $\text{V}/\mu\text{m}$ electric field in the hybrid films deposited at different temperatures of 500, 600 and 700 °C, are found to be 3.8×10^{-7} , 1×10^{-6} and $1 \times 10^{-3} \text{ A}/\text{cm}^2$, respectively. Thus, the value of E_T decreases and J increases with the increase of the deposition temperature of MWCNT-graphene like hybrid films. The corresponding values of β in the samples deposited at different temperatures of 500, 600 and 700 °C were found to be 1250, 3214 and 1600, respectively, which increase with the increase of deposition temperature up to 600 °C. The improved turn-on field at high temperature may be due to the unique rambutan like structure and the presence of graphene like sheets. These types of structures enhance local field in large amount

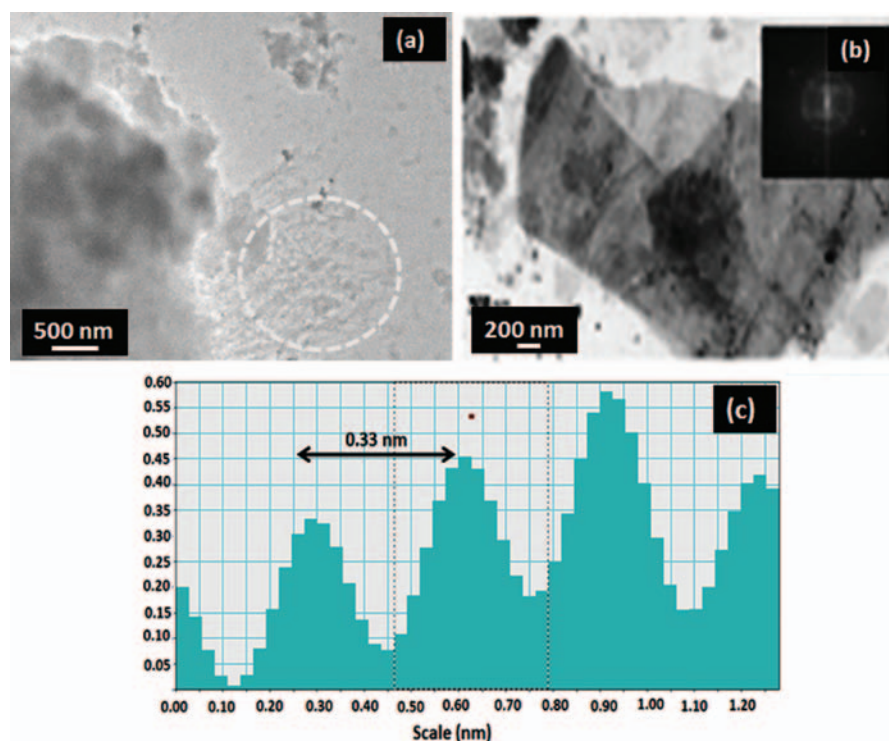


Fig. 7. (a) HRTEM image of MWCNT-graphene like hybrid film deposited at 700 °C, (b) sheet like graphene structure and FFT, and (c) interplaner distance of planes.

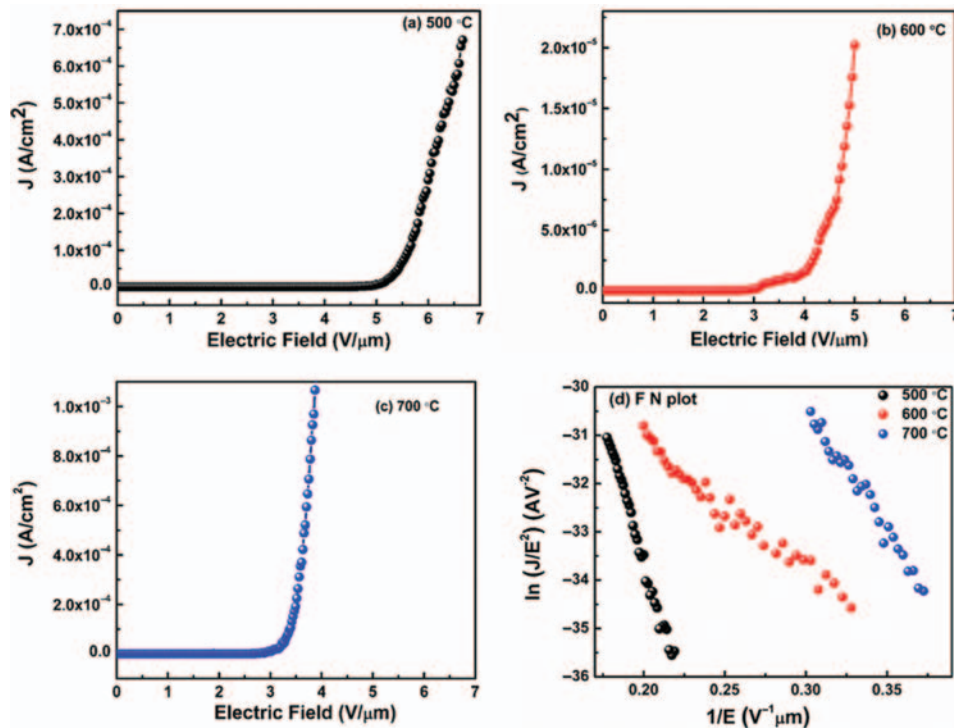


Fig. 8. Variation of emission current density (J) versus electric field (E) of MWCNT-graphene like hybrid films deposited at different temperatures of (a) 500, (b) 600, (c) 700 °C, and (d) their FN plots at different temperatures.

besides the external applied field which improve the field emission. CNT alone has also proved to be a promising field emitter material. Recently, direct deposition of the CNT on a bulk metallic substrate has proven to be a better field emitter due to the low contact resistance to substrate.^{31,32} Lahiri et al.³¹ also studied CNT deposition directly on the copper and argued that the direct deposition of field emitter on the metal substrate helps to extract any heat generated due to the presence of contact resistance. Neupane et al.³² synthesized CNT growth on the copper substrate with the help of nanosphere lithography and studied their field emission properties. Chen et al.³³ studied field emission properties of bare CNT and ammonia treated CNT and have found a very high turn-on field up to 11.93 V/μm (corresponding to 0.1 μA/cm² emission current density) and 8.84 V/μm with the plasma treatment. Pandey et al.³⁴ have studied the field emission properties of morphological disordered graphene, transferred to the silicon substrate and proposed a two barrier model with the first barrier from Si to graphene and the second barrier from graphene to vacuum. The two barrier model does not affect the present case as the films are directly deposited on the nickel substrate. Koh et al.¹⁴ while studying the field emission properties of CNT-graphene hybrid synthesized by electrophoretic deposition (EPD) technique, proposed that graphene improved the conductivity of CNT matrix acting as the connector particle between the CNTs as well as an additional local field enhancer in the surface region. The reason of better field emission of the

sample deposited at 700 °C in the present study may be due to the improved conductivity of CNT with the help of graphene and lower contact resistance between the substrate and CNTs, which also play an important role in the field emission. Nguyen et al.⁹ found the applicability of CNT-graphene hybrid in the flexible transparent conductor and field emitter and reported the improved sheet resistance of 420 ohm/sq with turn-on field up to 2.9 V/μm (corresponding to 10 μA/cm² emission current density) which is due to the lower contact resistance caused by the π - π interaction between graphene and CNT. Nguyen et al.³⁶ while studying the field emission on CNT-graphene hybrid material, have reported the improvement in the turn-on field from bare CNT (2.68 V/μm) to their hybrid counterpart (2.12 V/μm) as graphene facilitate electron transport from the nickel substrate to carbon nanotubes. On the basis of the reported literature,^{14,27-36} it can be concluded that the field emission properties of the carbon based materials are strongly dependent on the deposition parameters and film quality (adhesion with the substrate and contact resistance, etc.). For a material to be good field emitter, it should be highly conductive to provide the proper channel to the electron flow and should have sharp edges, vertical structure to provide high local field enhancement. Another factor directing the field assisted cold electron emission is the field enhancement factor (β) which depends totally on the sharp edges, miniaturizing the structure to nanoscale, vertical structures, large aspect ratio etc. The values of β may be related to the SEM

microstructure as shown in Figure 6. For the 500 °C hybrid film, SEM micrograph shows dispersed MWCNTs with lateral orientation, whereas the microstructure for 600 °C deposited film shows the dense MWCNTs and for 700 °C deposited film, the microstructure shows highly dense, rambutan like clustering.

Field emission not only depends on the field enhancement factor (which depends on the shape and aspect ratio of the emitter) but also depends on the work function of the emitter and contact resistance of the substrate to the film. In case of the CNT, local field screening of individual CNT due to the surrounding CNTs also play an important role. Further, moderate density of CNTs is preferred for the field emission. Highly dense and randomly oriented CNTs yield decreased local field due to quantum electric field screening effect in which nearby CNTs affect the field emission. Further, the electrons are emitted from the tips of CNTs, vertically aligned CNTs are better field emitter than the randomly oriented CNTs. The sample deposited at 600 °C shows randomly oriented CNTs compared to the sample deposited at 700 °C which shows clustered rambutan like structure but oriented vertically. These factors do not come in the formulation of field enhancement factor. These may be reasons for high current density and low turn-on field of sample deposited at 700 °C compared to the sample deposited at 600 °C besides of having high field enhancement factor.

3.5. Wettability Properties

Humidity has a speculative effect on the gas sensing properties like gas sensing of the deposited films and deteriorates the properties with the passage of time. For a sensor, it must be resistive to different environmental conditions in which humidity is the most effective. One important reason of the oxide based sensor to work at high temperature is that below 100 °C, the water molecules are adsorbed at the surface of sensing material which prevents the gas molecule to come in contact with the sensing material. Hsu et al.³⁷ have shown that the commercial metal oxide based sensor need high operating temperature (100 °C) to remove the humidity effect. Once water molecules are absorbed, heating or UV exposure is the only treatment to remove the water molecule which may deteriorate the sensor performance. Self-cleaning of the film has an important relation to the contact angle of water with the film.³⁸ Cantalini et al.³⁹ have shown the negligible effect on CNT in a 80% humid environment and performed the experiment at an elevated temperature of 165 °C. To check the humid resistive nature of the film, the wettability properties of the sample deposited at 700 °C have been measured by the contact angle measurement. Hydrophobicity is the property of material to remove water. Figure 9 shows the wettable properties of the bare nickel and MWCNT-graphene like hybrid film on nickel with the shape of a water droplet. It is evident from the Figure that the bare nickel has a

contact angle of 77.8°, whereas the contact angle increases up to 128.4° in MWCNT-graphene like hybrid film coated on nickel showing the hydrophobic nature of the film. The contact angle can be further enhanced by the surface treatment of the film. Some et al.¹⁹ have studied the hydrophobic and hydrophilic nature of graphene oxide (GO) and reduced graphene oxide (rGO) and reported the contact angle as 48.8 and 79.3°, respectively.

3.6. Ammonia Sensing

For the sensing measurement, we have etched the base nickel substrate and transferred the MWCNT-graphene like hybrid film on the glass substrate. The ammonia gas sensing measurement has been performed on the MWCNT-graphene like hybrid film deposited at 700 °C at different ppm levels of ammonia in nitrogen as well as air environments (Figs. 10(a)–(d)). Figure 10(a) shows the ammonia gas sensing response of MWCNT-graphene like hybrid film sensor deposited at 700 °C with the increase of ppm level of ammonia in the nitrogen environment. It is evident from the figure that there is a repeatable response and recovery for ammonia gas. CNT and graphene shows p-type behavior in the ambient condition with the hole as majority of charge carriers.¹⁶ Ammonia behaves as a strong reducing or electron donating gas evacuating/neutralizing the majority charge carrier (holes), which results in the increase of electrical resistance of the film as evident from Figure 10(a). It is evident from the Figure 10(a) that the sensor recovers more than 90% of the original baseline in a very short time when purged with nitrogen without having any extra treatment e.g., heating or exposed to infrared radiation etc. The sensor shows the recoverable nature with the consequent absorption/desorption cycle. The gas sensing response of the film deposited at 700 °C measured in the air ambient is shown in Figure 10(b). Moreover, it has been observed that the sensor does not recover the base line as in the case of nitrogen environment, which may be due to some stronger interaction of ammonia with the hybrid film in air ambient.

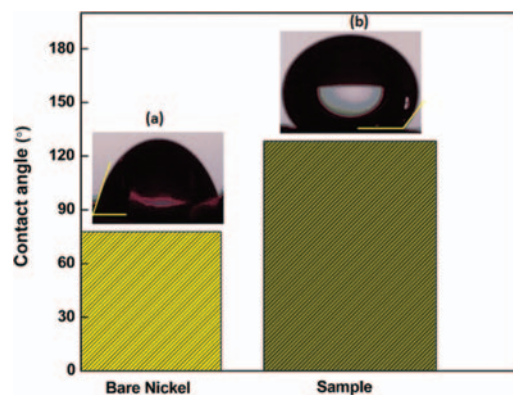


Fig. 9. Wettability of (a) bare Ni substrate and (b) MWCNT-graphene like hybrid film deposited at 700 °C.

On the exposure of p-type materials with electron donating ammonia, the charge compensation process can take place via either electron or proton transfer between the sensor material and the gas. The recovery of the prepared sample depends on the type of interaction between the sample and gas molecules under analysis. It is only possible for the weak interaction. On the other hand, when the interaction of the gas molecules under analysis with the sensor material is stronger or some nucleophilic reaction takes place with the formation of hydroxyl (OH⁻) groups, then the sample fails to attain its original state with the change of environment from ammonia to air and the process becomes irreversible. In the present study, we have observed around 80–90% recovery for air testing as it is clear that the sensor has not recovered its original baseline. It has been observed that the electrical resistance of the sample is not much affected by the ambient air environment or the presence of humidity in the air. The change in electrical resistance in both the dry nitrogen as well as in the air environment remains almost the same. This could be due to the hydrophobic nature of the samples as observed from the wettability test. It is reported in the literature that the humidity and ammonia act in the opposite manner on the conductivity of a sensing material.⁴⁰ Humidity acts as an acceptor and ammonia acts as a donor. Thus, the humidity may cancel out the effect of ammonia. Humidity can also be added up to the ammonia effect if it produces a swelling type of effect, which may cause the bond angle

and bond length alteration and hence increase in the electrical resistance. But, we have not observed much effect of testing environment on the sensor performance. Since the sample is hydrophobic, thus, humidity effect can be ignored. Zhao et al.⁴¹ showed that there is no significant change in the density of states in the bare CNT and ammonia doped CNT which indicates that the charge transfer is not substantial. Figure 10(c) also shows the exponential fitting of the conductance curve for the response and recovery of the MWCNT-graphene like hybrid film sensor at fixed 100 ppm ammonia at room temperature with the help of Eqs. (3) and (4).

$$G(t)_{\text{response}} = G_0 + G_1[\exp(-t/\tau_{\text{response}})] \quad (3)$$

$$G(t)_{\text{recovery}} = G_0 + G_1[\exp(t/\tau_{\text{recovery}})] \quad (4)$$

Where G_0 and G_1 are the fitting parameters and τ_{response} and τ_{recovery} are the response and the recovery time of the sensor. For a good sensing property, both the response and recovery time must be low. From the fitting curve, the response and recovery time were found to be 40 and 96 s, respectively, showing very low values. No saturation of the time response was observed in the present study as we have limited the inserting and flushing time of 200 and 300 s, respectively. However, when we have increased the ammonia exposure time up to 400 s and flushing time of 800 s at 300 ppm of ammonia, the sensor almost attend the saturation in the electrical resistance of

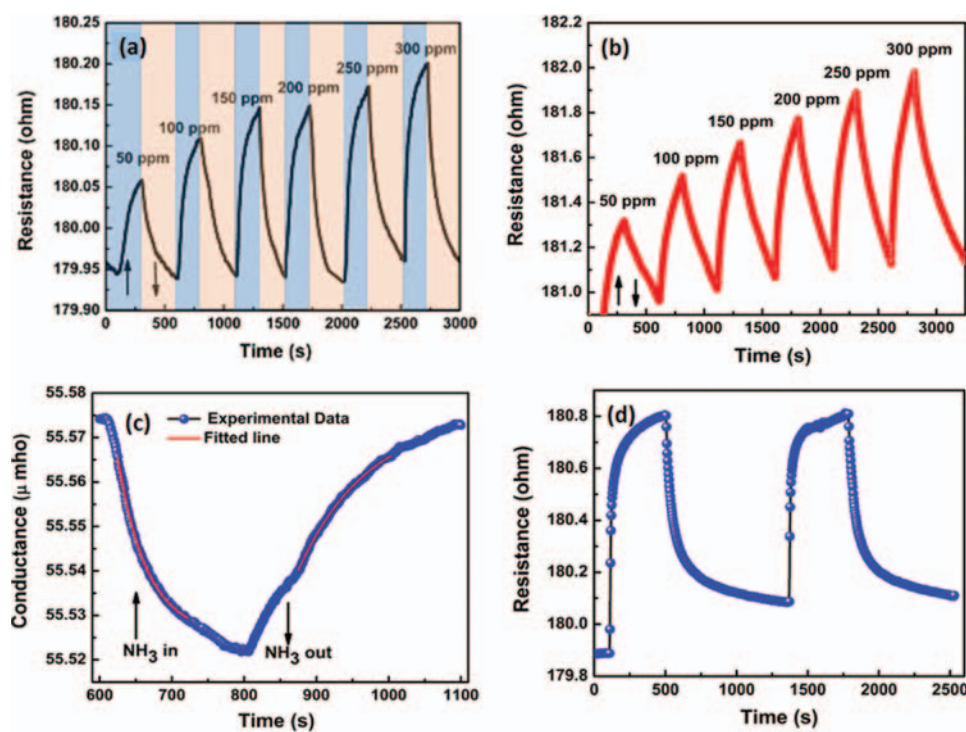


Fig. 10. Ammonia gas sensing response curve of MWCNT-graphene like hybrid film deposited at 700 °C for (a) the nitrogen environment, (b) the air ambient at different ppm levels (50–300 ppm), (c) exponential fitting for response and recovery time at 50 ppm ammonia gas in the nitrogen environment, and (d) sensing response recorded for longer duration at 300 ppm of ammonia gas in the air ambient.

the sensor (Fig. 10(d)). The activation energy required for the molecular desorption of gas is higher than the thermal energy of molecules at room temperature, so higher temperature is needed for the complete desorption of gas molecules which makes the sensor more complex and costly.⁴² However, the recovery time of the ammonia gas sensor in the present study is very low. The low value of response and recovery time may be related to the physisorption by Vander wall force of ammonia on the surface. Due to the π electron system in sp^2 based carbon nanostructure, the electrical properties are very sensitive to the charge transfer by adsorbed molecules. Generally, CNT and graphene behave as p-type materials at room temperature with the hole as majority of charge carriers. Ammonia being a reducing gas donates electron to the CNT and lowers the majority charge carrier and thus increasing the resistance in the presence of gas. One advantage of the CNT-graphene film over the composite film as sensor is that it can be transferred easily to the flexible substrate for the flexible gas sensor. Recently, Pandey et al.⁴³ developed a very simple and cost effective technique for the room temperature ammonia gas sensing by silver nanoparticle/guar gum based composite. They claimed that the sensor based on guar gum/silver nanoparticle composite was flexible and ultrasensitive for the ammonia gas. It consisted of ideal properties of the sensor as a room temperature operative, working in the ambient environment, no external factor required for the response and recovery e.g., ultraviolet radiation, heating, low detection limit with the high sensitivity and reproducibility, fast response/recovery with low cost. Lee et al.⁴⁴ studied the sensing properties of gold nanoparticle decorated CNT as flexible and transparent ammonia gas sensor and found a high recovery time. Nguyen et al.⁴⁵ studied ammonia sensing by CNT decorated with cobalt nanoparticle at room temperature and found response time 30–50 s with recovery time of 200 s. Tran et al.⁴⁶ also studied graphene-silver nanowire composite for ammonia sensing and found high response time of 200 s and recovery time 60 s with the purging of the inert gas argon instead of air. Johnson et al.⁴⁷ reported ammonia sensing of the CNT, graphitic nanoribbon film and found recovery time of 90, 115 s, respectively. Llobet¹⁷ reviewed the state of the art for electrical gas sensors using carbon nanomaterial, identifies the bottlenecks for their commercialization and some breakthroughs and gave an outlook with challenges and opportunities.

4. CONCLUSION

MWCNT-graphene like hybrid films have been grown at different temperatures (500–700 °C) at a fixed pressure of 20 Torr by MW PECVD technique. Higher wavelength shifting of G peak in the Raman spectra confirmed the presence of graphene like carbon sheets along with MWCNT. The value of E_T was found to be 4.7, 3.6 and

2.7 V/ μm for the MWCNT-graphene like hybrid films deposited at 500, 600 and 700 °C, respectively. The lowest value of $E_T = 2.7$ V/ μm accompanied with the highest value of $J = 1$ mA/cm² (at 3.8 V/ μm electric field) have been obtained in the hybrid film deposited at 700 °C. The ammonia gas sensor showed the fast response and recovery time of 40 and 96s, respectively, in the hybrid film deposited at 700 °C. The hydrophobic nature of the film makes the films suitable for gas sensing applications even in the humid environments. Thus, the field emission behavior accompanied with the good response and recovery time in ammonia gas sensing at room temperature is demonstrated in the MWCNT-graphene like hybrid films.

Acknowledgments: The authors are grateful to Professor R. C. Budhani, Director, CSIR-National Physical Laboratory, New Delhi (India) for his kind permission to publish this paper. They wish to thank to Mr. K. N. Sood for providing the SEM micrograph, to Dr. A. M. Biradar for providing the contact angle measurement and to Mr. Jagdish Chand for providing the technical help. Mr. Atul Bisht and Mr. Ajay Kumar Kesarwani are grateful to the University Grant Commission (UGC) and Council of Scientific Industrial Research (CSIR), Government of India, respectively, for the financial assistance during the course of this work.

References and Notes

1. S. Park, M. Vosguerichian, and Z. Bao, *Nanoscale* 5, 1727 (2013).
2. L. Hu, D. S. Hecht, and G. Grüner, *Chem. Rev.* 110, 5790 (2010).
3. A. K. Geim and K. S. Novoselov, *Nat. Mater.* 6, 183 (2007).
4. K. S. Novoselov, V. I. Falko, L. Colombo, P. R. Gellert, M. G. Schwab, and K. Kim, *Nature* 490, 192 (2012).
5. O. S. Panwar, A. K. Kesarwani, S. R. Dhakate, B. P. Singh, R. K. Rakshit, A. Bisht, and S. Chockalingam, *J. Vac. Sci. Technol. B* 31, 040602 (2013).
6. A. K. Kesarwani, O. S. Panwar, S. Chockalingam, A. Bisht, S. R. Dhakate, B. P. Singh, A. K. Srivastava, and R. K. Rakshit, *Sci. Adv. Mater.* 6, 10 (2014).
7. X. Dong, B. Li, A. Wei, X. Cao, M. B. Chan-Park, H. Zhang, L. J. Li, W. Huang, and P. Chen, *Carbon* 49, 2944 (2011).
8. X. Zhu, G. Ning, Z. Fan, J. Gao, C. Xu, W. Qian, and F. Wei, *Carbon* 50, 2764 (2012).
9. C. Kang, R. Baskaran, J. Hwang, B. C. Ku, and W. Choi, *Carbon* 68, 493 (2014).
10. M. Taniguchi, H. Nagao, M. Hiramoto, Y. Ando, and M. Hori, *Diamond Relat. Mater.* 14, 855 (2005).
11. G. Atthipalli, R. Epur, P. N. Kumta, M. Yang, J. K. Lee, and J. L. Gray, *J. Phys. Chem. C* 115, 3534 (2011).
12. J. H. Deng, G. A. Cheng, R. T. Zheng, B. Yu, G. Z. Li, X. G. Hou, M. L. Zhao, and D. J. Li, *Carbon* 67, 525 (2014).
13. J. H. Deng, R. T. Zheng, Y. M. Yang, Y. Zhao, and G. A. Cheng, *Carbon* 50, 4732 (2012).
14. A. T. T. Koh, T. Chen, L. Pan, Z. Sun, and D. H. C. Chua, *J. Appl. Phys.* 113, 174909 (2013).
15. I. Sayago, H. Santos, M. C. Horrillo, M. Aleixandre, M. J. Fernández, E. Terrado, I. Tacchini, R. Aroz, W. K. Maser, A. M. Benito, M. T. Martínez, J. Gutiérrez, and E. Muñoz, *Talanta* 77, 758 (2008).
16. S. Mao, G. Lu, and J. Chen, *J. Mater. Chem. A* 2, 5573 (2014).

17. E. Llobet, *Sens. Actuators B* 179, 32 (2013).
18. L. Yuan, T. Hyodo, Y. Shimizu, and M. Egashira, *Sensors* 11, 1261 (2011).
19. S. Some, Y. Xu, Y. Kim, Y. Yoon, H. Qin, A. Kulkarni, T. Kim, and H. Lee, *Sci. Rep.* 3, 01868 (2013).
20. K. Bradley, J. C. P. Gabriel, M. Briman, A. Star, and G. Grüner, *Phys. Rev. Lett.* 91, 218301 (2003).
21. A. C. Ferrari and D. M. Basko, *Nat. Nano* 8, 235 (2013).
22. R. Saito, M. Hofmann, G. Dresselhaus, A. Jorio, and M. S. Dresselhaus, *Adv. Phys.* 60, 413 (2011).
23. M. S. Dresselhaus, A. Jorio, A. G. S. Filho, and R. Saito, *Phil. Trans. R. Soc. A* 368, 5355 (2010).
24. A. C. Ferrari, J. C. Meyer, V. Scardaci, C. Casiraghi, M. Lazzeri, F. Mauri, S. Piscanec, D. Jiang, K. S. Novoselov, S. Roth, and A. K. Geim, *Phys. Rev. Lett.* 97, 187401 (2006).
25. G. Tong, F. Liu, W. Wu, F. Du, and J. Guan, *J. Mater. Chem. A* 2, 7373 (2014).
26. M. Zheng, K. Takei, B. Hsia, H. Fang, X. Zhang, N. Ferralis, H. Ko, Y. L. Chueh, Y. Zhang, R. Maboudian, and A. Javey, *Appl. Phys. Lett.* 96, 063110 (2010).
27. R. H. Fowler and L. Nordheim, *Proc. R. Soc. A London* 119, 173 (1928).
28. O. S. Panwar, N. Rupesinghe, and G. A. J. Amaratunga, *J. Vac. Sci. Technol. B* 26, 566 (2008).
29. O. S. Panwar, M. A. Khan, B. S. Satyanarayana, R. Bhattacharyya, B. R. Mehta, S. Kumar, and Ishpal, *J. Vac. Sci. Technol. B* 28, 411 (2010).
30. O. S. Panwar, S. Kumar, S. S. Rajput, R. Sharma, and R. Bhattacharyya, *Vacuum* 72, 183 (2004).
31. I. Lahiri, R. Seelaboyina, J. Y. Hwang, R. Banerjee, and W. Choi, *Carbon* 48, 1531 (2010).
32. S. Neupane, M. Lastres, M. Chiarella, W. Li, Q. Su, and G. Du, *Carbon* 50, 2641 (2012).
33. G. Chen, S. Neupane, W. Li, L. Chen, and J. Zhang, *Carbon* 52, 468 (2013).
34. S. Pandey, P. Rai, S. Patole, F. Gunes, G. D. Kwon, J. B. Yoo, P. Nikolaev, and S. Arepalli, *Appl. Phys. Lett.* 100, 043104 (2012).
35. D. D. Nguyen, N. H. Tai, S. Y. Chen, and Y. L. Chueh, *Nanoscale* 4, 632 (2012).
36. D. D. Nguyen, R. N. Tiwari, Y. Matsuoka, G. Hashimoto, E. Rokuta, Y. Z. Chen, Y. L. Chueh, and M. Yoshimura, *Appl. Mater. Interf.* 6, 9071 (2014).
37. L. C. Hsu, T. Ativanichayaphong, H. Cao, J. Sin, M. Graff, and H. E. Stephanou, *Sens. Rev.* 27, 121 (2007).
38. R. Wang, K. Hashimoto, A. Fujishima, M. Chikuni, E. Kojima, A. Kitamura, M. Shimohigoshi, and T. Watanabe, *Adv. Mater.* 10, 135 (1998).
39. C. Cantalini, L. Valentini, I. Armentano, L. Lozzi, J. M. Kenny, and S. Santucci, *Sens. Actuators B* 95, 195 (2003).
40. C. H. Kim, S. W. Yoo, D. W. Nam, S. Seo, and J. H. Lee, *IEEE Electron Device Lett.* 33, 1084 (2012).
41. J. Zhao, A. Buldum, J. Han, and J. P. Lu, *Nanotechnol.* 13, 195 (2002).
42. R. Ghosh, A. Midya, S. Santra, S. K. Ray, and P. K. Guha, *ACS Appl. Mater. Interf.* 5, 7599 (2013).
43. S. Pandey, G. K. Goswami, and K. K. Nanda, *Sci. Rep.* 3, 02082 (2013).
44. K. Lee, V. Scardaci, H. Y. Kim, T. Hallam, H. Nolan, B. E. Bolf, G. S. Maltbie, J. E. Abbott, and G. S. Duesberg, *Sens. Actuators B* 188, 571 (2013).
45. L. Q. Nguyen, P. Q. Phan, H. N. Duong, C. D. Nguyen, and L. H. Nguyen, *Sensors* 13, 1754 (2013).
46. Q. T. Tran, T. M. H. Huynh, D. T. Tong, V. T. Tran, and N. D. Nguyen, *Adv. Nat. Sci.: Nanosci. Nanotechnol.* 4, 045012 (2013).
47. J. L. Johnson, A. Behnam, Y. An, S. J. Pearton, and A. Ural, *J. Appl. Phys.* 109, 124301 (2011).